Aggregation of FeCl2 Clusters in Supercritical Water Investigated by Molecular Dynamics Simulations

ARTICLE *in* THE JOURNAL OF PHYSICAL CHEMISTRY B · SEPTEMBER 2008

Impact Factor: 3.3 · DOI: 10.1021/jp710156b

1 AUTHOR:

Bjørn Kvamme
University of Bergen
364 PUBLICATIONS **1,647** CITATIONS

SEE PROFILE

Aggregation of $FeCl_2$ Clusters in Supercritical Water Investigated by Molecular Dynamics Simulations

Norbert Lümmen* and Bjørn Kvamme

Department of Physics and Technology, University in Bergen, Allégaten 55, N-5007 Bergen, Norway

Received: October 19, 2007; Revised Manuscript Received: July 24, 2008

We have carried out molecular dynamics (MD) simulations of the aggregation of $FeCl_2$ clusters in supercritical water. The particle formation in systems of 2048 water molecules (rigid SPC/E-model) and 120 Fe^{2+} ions and 240 Cl^- ions has been investigated for 250 ps at five different state points at temperatures from 798 to 873 K and system densities from 0.18 g/cm^3 to 0.13 g/cm^3. We describe the particle growth by means of properties of the largest cluster in a system as well as cluster size averaged and time averaged observables. From preexisting or immediately formed units of $Fe^{2+}-Cl^-$, $Fe^{2+}-Cl^-_2$, $Fe^{2+}-Cl^-_3$ etc., the further growth of clusters is dominated by aggregation of such small building blocks. Clusters up to 10 ions in size with large charge imbalances are found during the growth process while a balanced positive to negative charge ratio is found on the average with time and cluster size development. Water molecules are found within the $FeCl_2$ clusters during the whole time interval covered by the simulations, which is in agreement with the existence of crystal water in $FeCl_2$ crystals grown from aqueous solutions. The radial distribution functions obtained from the simulation data are in good agreement with experimental results of slightly distorted $FeCl_2 \cdot 4H_2O$ crystals.

Introduction

Supercritical water (SCW), that is water above its critical point ($T_c = 647$ K, $p_c = 22$ MPa, and $\rho_c = 0.322$ g/cm^3),[1] shows a number of different properties compared to water at ambient conditions. For example, the dielectric constant changes from 80.2 to 1.5 at 823 K and 25 MPa.[2] The change in water structure due to a smaller degree of hydrogen bonded structure changes the solvation properties of water. While experiments have shown that ions tend to aggregate under such conditions,[3] non-polar molecules are dissolved in SCW. As the solvation properties can be controlled by the applied temperature and pressure above the critical point SCW is, like many other supercritical fluids, a suitable solvent in materials processing, pharmacy and food industry.[4−7]

Supercritical water oxidation (SCWO) is a technology to purify water contaminated with organic waste. Non-polar organic molecules, which are soluble in supercritical water, are broken down into smaller less problematic or nontoxic molecules in the presence of molecular oxygen.[2] However, halogenated organic waste is difficult to treat with this process as salt particles are formed. These solid salt particles precipitate out from the fluid and may cover reactor walls and may lead to plugging of pipelines. The same applies to desalination during fresh water production from seawater which is also an interesting application of SCW with increasing potential. Although new reactor designs to a certain extent can cope with the problem of plugging,[8,9] salt precipitation is still a problem within this technology. Molecular simulations of the particle formation process can assist in the development of more fundamental understanding of the dynamics involved and may as such assist in understanding the problem, and contribute in the search for new solutions that subsequently can lead to better reactor designs and/or process designs. A way to achieve this is by including detailed findings about processes at the molecular level into models which describe reactions and flow on larger length scales than those used in molecular simulations. Simulation of reactions and flow in a SCWO reactor by means of computational fluid dynamics are one example.

Natural hydrothermal fluids are rich in ionic species[10−12] like, for example, Fe^{2+} and Mn^{2+}. While seawater circulates through porous seafloor, it changes its composition with changing temperature and pressure due to exchange processes with the surrounding rock.[13] Below water depths of more than 2800 m the pressures are high enough for seawater to attain supercritical state if a heat source like intrusive basalt is present. This can lead to natural salt particle formation and the formation of (sub-) seafloor ore deposits like metal-rich brines or metalliferous sediments.[14] The aggregation of NaCl due to subsurface boiling of critical seawater was recently verified in experiment and computer simulations by Hovland et al.[15,16] It is most likely, that this process also leads to large aggregates and deposits of metal salts, if the hydrothermal fluid feed is rich in metal ions. A technological application of $FeCl_2$ is, for example, the wet chemical synthesis of FePt nanoparticles that can be used as magnetic material for a new generation of ultra high density magnetic storage devices.[17]

In this work we study the formation of $FeCl_2$ nanoparticles from supercritical water in order to investigate such particle aggregation for one of the most abundant ionic species in deep sea hydrothermal fluids. Simulation studies of other metal salts in water have been done by several groups, of which we only mention a limited number of recent examples. The work on Cu^+ by Sherman[18] is one example. He investigated the stability of Cu^+-Cl^- complexes in aqueous solutions containing additional NaCl at temperatures between 25 and 450 °C. Harris et al.[19] studied aqueous $ZnCl_2$ solutions of 222 SPC/E water[20] molecules containing 4 to 36 $ZnCl_2$ molecules by molecular dynamics simulations at high pressure and temperature. At high Cl^- concentration they found no $Zn^{2+}-Cl^-$ complexes contain-

* Corresponding author. E-mail: norbert@ift.uib.no.

10.1021/jp710156b CCC: $40.75
Published on Web 09/09/2008

ing more than one Zn^{2+} ion. However, clusters of containing several Zn^{2+} and $Cl-$ ions were found at higher temperatures. MD simulations were also used to study the nucleation of AgBr in water by Shore and co-workers.[21] As $Ag_{18}Br_{18}$ clusters formed at 325 K in 256 water molecules were found to be in a disordered structure a two step cluster formation process was suggested. In this process it is assumed, that first a disordered structure is attained by a growing salt particle that later transforms into a regular and ordered crystal structure. Many groups have covered the field of alkali-metal salt formation in aqueous solution at different state conditions like, for example, NaCl by Reagan et al.[22] Solutions with 21 wt % NaCl (17 ion pairs in 216 water molecules) were investigated at a pressure of 25 MPa and temperatures up to 727 °C to study the solution structure and ion association ion a dense brine. Oversaturated NaCl and CsF solutions were the subject of a molecular dynamics simulation study carried out by Ohtaki and Fukushima.[23] At a constant temperature of 298 K ion association was observed to take place within 12−18 ps in systems with high cation:anion:water molecules ratios of 56:56:336 to 127:127:194.

Methods

We closely follow the procedure we employed in our recently published study on NaCl-particle formation in supercritical water.[24] The molecular dynamics (MD) simulations program package M.DynaMix 4.3[25] was chosen as the basic platform. The trajectory analysis tool *tranal* included in this package was modified to allow for the detection of clusters by means of the Stillinger criterion.[26] This simple geometric criterion marks two atoms belonging to the same cluster if they lie within a certain given distance from each other. These distance criteria are taken as the first minima in corresponding radial distribution functions which have to be generated from the molecules' and ions' trajectories before the cluster analysis can be started. In the simulations a time step of 1 fs was used to integrate the Newton's equations of motion by a simple leapfrog algorithm.[27]

During particle formation, potential energy is locally converted into kinetic energy, which leads to a heating up of those atoms or ions involved in the collision. If the heating up is too strong, then the aggregate is likely to be unstable and to decay. This can be the case if the relative velocity to each other was initially high, or if a large amount of potential energy is converted into kinetic energy due to a strong interaction. The use of a heat bath is then often necessary to observe particle formation. This heat bath removes condensation heat so that particles are more likely to be formed than would otherwise be the case without a heat sink. In molecular simulations this is usually done through so-called thermostats. The schemes of Berendsen et al.,[28] Andersen,[29] Nosé,[30] and Nosé−Hoover[31] are examples for different homogeneous methods of coupling a system to a heat bath within a molecular simulation. Homogeneous means that all particles in the system are treated equally in terms of adjusting the system temperature by rescaling the particle velocities. While condensation in weakly interacting systems, like Lennard-Jones argon for example, can be observed without coupling to a heat bath at all,[32] a need for a thermostat to remove the released heat during particle aggregation gets more and more necessary with increasing interaction strength. Erhart and Albe[33] have investigated in detail different thermostatting techniques with respect to their applicability in particle formation simulations. They found that the direct application of homogeneous thermostat techniques onto strongly interacting species undergoing nucleation and growth at low system densities leads to unrealistic particle morphologies and crystal structures. Erhart and Albe[33] came to the conclusion that the most suitable way of temperature control in a system undergoing particle formation is to use an additional substance which does not condense at the given state conditions. The heat of the condensing species is transferred to the inert, noncondensing species, just by collisions. The inert species can then be treated by one of the homogeneous thermostatting schemes mentioned above. This method of temperature control is closer to the experimental situation where particles are usually grown in a solvent or a carrier gas atmosphere. Westergren et al.[34] have carried out a detailed investigation of the properties of such a heat bath thermostat based on the Lennard-Jones potential as interaction model. A more recent study on the effect of amount of inert gas used in the heat bath thermostat on nucleation rates was published by Wedekind et al.[35] We have successfully applied this way of temperature control in our previous study of NaCl aggregation in supercritical water.[24] Other examples of its application are simulations of condensation in supersaturated vapors of, for example, water,[36] and strongly interacting systems like zinc[37] and iron−platinum.[38]

As the system density in the investigated supercritical systems is low and lies somewhere between that of the liquid and vapor phase an important precondition for applying a homogeneous thermostat to the ions and the water molecules at the same time is not necessarily fulfilled. Application of the thermostat coupling only to the solvent medium, i.e., the water molecules, counteracts a potential direct influence on the particle formation process of the ionic species through the thermostat mechanism. This is why we chose to let a Nosé−Hoover thermostat[30,31] act on the water molecules only in all simulations with ion aggregation. Analogous to the studies of salt precipitation from supercritical water by Hovland et al.[16] and our previous study on NaCl aggregation in supercritical water[24] the Nosé-Hoover thermostat parameter was chosen to be 100 fs. Brodholt[39] used value of 500 fs in his investigation on concentration effects of NaCl in SPC/E water at high temperatures and pressures. A too large value of the thermostat parameter can lead to initially large damped oscillations in the temperature after temperature changes, in which the frequency will increase with increasing parameter value. In our case a value of 500 fs lead to this behavior with oscillations with a period of a few picoseconds in the water temperature which disappeared on the time scale of around 25 ps. The temperature of the ionic species coupled to these oscillations when their temperature reached the temperature of the heat bath before this point after their temperature had initially increased due to aggregation. Using the lower value of 100 fs did not result in the described temperature oscillations of the heat bath and the mentioned coupling of the ion temperature to them.

To prepare start configurations for the particle formation simulations, systems of 2048 water molecules containing 120 Fe^{2+} ions and 240 Cl^- ions in cubic simulation boxes were equilibrated at ambient conditions (298 K, 1.3 g/cm^3) for 250 ps. This was also done in order to randomize the distribution of the ions among the water molecules instead of starting from a random distribution of water molecules and ions on a regular grid. As ion aggregation does not take place at these conditions we applied velocity scaling to all molecules and ions in the system to keep the system temperature constant. The large amount of ions was chosen in order to gain good statistics in the analysis of aggregation rates.[40] The amount of ions yields a $FeCl_2$ content of 29.2 wt %. This corresponds to an ion to water molecule ratio of 0.176 (=360 ions/2048 water molecules). A

TABLE 1: Parameters for the Lennard-Jones part of Fe^{2+} Interaction Potentials

authors	ϵ/(kJ/mol)	σ/nm
Lümmen, Kvamme (this work)	0.36132	0.2
Babu, Lim[44]	0.11053	0.2403

slightly lower ion:water ratio of 0.156 was used in our investigation on NaCl aggregation[24] with 20.2 wt % NaCl. These values are comparable to weight fractions and ion:water ratios employed by other groups. Twenty-one wt % NaCl solutions (ion:water ratio of 0.157) were studied by Reagan et al.[22] and the values in Brodholt's investigation ranged up to 23 wt % with ion:water ratio at 0.188.[39] But there are also examples of much larger ion to water molecule ratios. The largest amount of $ZnCl_2$ in water studied by Harris et al.[19] was a 53.7 wt % solution with an ion:water ratio of 0.486. The CsF solutions investigated by Ohtaki and Fukushima[23] ranged from 42.3 wt % and 0.333 to 58.4 wt % and 1.31. To summarize, the quantity of ions and water molecules we selected is well suited for our purpose of showing the applicability of the chosen methods to investigate particle formation of divalent metal salts from supercritical water and obtaining detailed results of the particle growth at the molecular scale.

In both preparatory simulation runs, as well as in the particle formation simulations, standard MD-simulation techniques like minimum image convention and periodic boundary conditions were used. Within M.DynaMix 4.3[25] the intermolecular forces of the Lennard-Jones type are cut beyond a cutoff radius, which we set to 1.0 nm, and set to zero beyond the cutoff. The Ewald-summation method[27] (real part cutoff at 1.0 nm, damping constant $= \pi/10$) was applied to treat the long-range forces originating from the partial charges on the water molecules and the ionic charges. The ion and molecule positions and velocities as well as system pressure, system temperature and the temperatures of each species were stored every 0.2 ps for later analysis.

The water−water interaction was modeled by the rigid extended simple point charge (SPC/E) model[20] while using the SHAKE algorithm[41] to keep the internal bond lengths fixed. The SPC/E model was found to give good results in several studies on salt containing solutions at high temperatures and pressures, for example in the ones by Harris et al.[19] and Smith and Dang.[42] For the ionic and water-ion interaction we employed a combination of Lennard-Jones potential and Coulomb potential. We used the parameters of Smith and Dang[42] for Cl^- and a fit of the empirical pair potential for Fe^{2+} by Curtiss et al.[43] to the combined Lennard-Jones/Coulomb potential. The parameters used are given in Table 1. During the analysis of our simulation runs, the Fe^{2+} parameters by Babu and Lim[44] became available. Although the values for both potential trough and width differ from ours a comparison showed, that there are no significant differences in the dynamics of the particle formation process and radial distribution functions, when using either the parameter set by Babu and Lim or ours. For comparison we carried out an analysis of the radial distribution functions and coordination number of a single Fe^{2+} ion in a system of 512 SPC/E water molecules at 298 K and 1 g/cm^3 system density for 25 ps after an initial equilibration period of 25 ps. Both our parameters and those by Babu and Lim showed agreement with the radial distribution function in the work by Curtiss et al.[43] and the experimental value of 6 for the coordination number of the Fe^{2+} ion in the first solvation shell.[43] The only slight differences were found in the location of the first maximum in the radial O−Fe^{2+} distribution function and the behavior of the coordination number beyond the second coordination shell which can be seen in Figure 1. With a spatial resolution of 0.001 nm the first O−Fe^{2+} maximum was found at 0.2085 nm with the parameters of Babu and Lim[44] while it was at 0.2045 nm with our parameters.

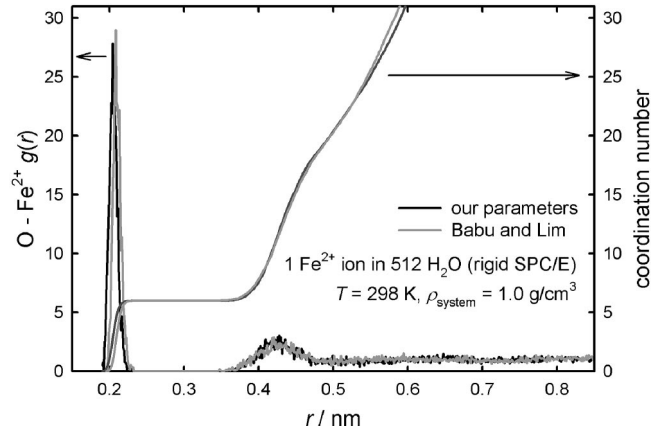

Figure 1. Comparison of radial distribution functions $g(r)$ and coordination number for a single Fe^{2+} ion in 512 SPC/E water molecules using the two Lennard-Jones parameters sets given in Table 1. The $g(r)$ curves have been determined from 250 configurations.

Results

After equilibrating the systems for 250 ps at ambient conditions (298 K, 1.3 g/cm^3) nine particle formation simulation runs were carried out for 250 ps at each of the five different state points. It turned out, that it is not necessary to simulate these systems beyond this time range. The ionic aggregation and most of the structural development of the clusters happen on this time scale. The heat bath temperature (T_{hb}) and system density combinations 798 K and 0.18 g/cm^3, 835 K and 0.16 g/cm^3, and 873 K and 0.13 g/cm^3 were chosen to yield a system pressure of around 25 MPa at the end of the particle formation during the simulation runs. In addition two combinations: 1) 835 K and 0.18 g/cm^3 and 2) 835 K and 0.13 g/cm^3 were chosen in order to visualize the effects of higher and lower system density in the vicinity of one of the three first chosen state points. The state points were selected analogue to our study on NaCl aggregation.[24] The same heat bath temperatures were used and the system densities were chosen to yield a system pressure of around 25 MPa at the end of the particle formation. Compared to the simulation volume during equilibration, the change to the supercritical conditions enlarges this volume by a factor of about 7.2 (0.18 g/cm^3) to 10.0 (0.13 g/cm^3). Such an instant change to metastable state conditions to induce particle formation is a standard technique used in molecular dynamics simulations of nucleation and growth. In this way one prevents nucleation and growth from taking place already before the state points of interest are reached which would happen if one applied a slower and more gradual change in state conditions. Examples of the application of this scheme are the investigation of nucleation of argon[35] and the study of nucleation of water by Yasuoka and Matsumoto.[36] We have found no dependence of the dynamics after the change in state conditions on the use of a lower (298 K) or higher (923) K system temperature during equilibration.

The first step in each simulation is the change from ambient conditions over to the given supercritical conditions. The particle coordinates are scaled in the same way as the size of the simulation volume. The rescaling of the temperature by means

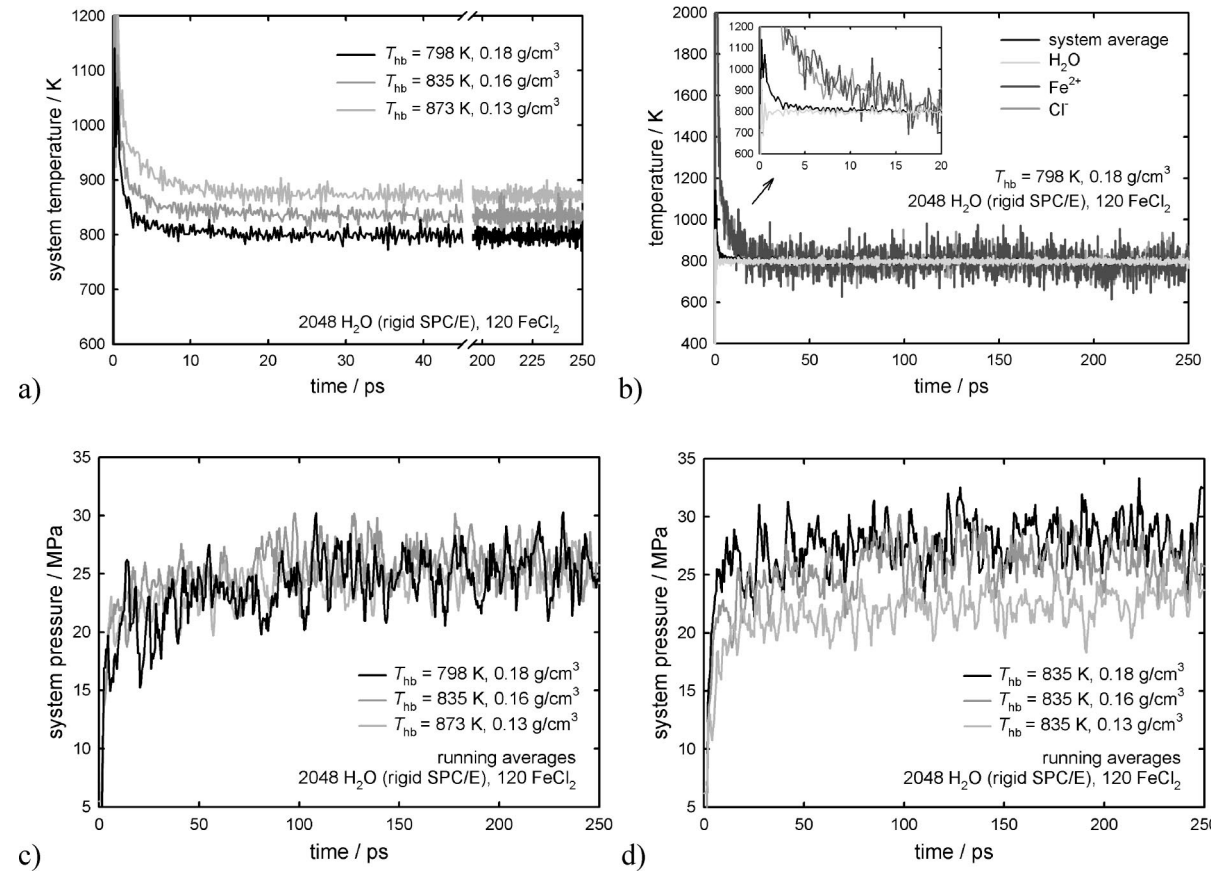

Figure 2. (a) Time development of the system temperature for single simulation runs at three different state points. (b) Time development of the temperature of the single species within a single simulated system together with the curve of the average system temperature. The inset shows a close up on the first 20 ps of the temperature development. (c) Time development of the system pressure for single simulation runs at three different state points. Running averages are shown. (d) Same as part c but for systems at the same heat bath temperature but different system densities. Temperatures given in the legends are the temperature of the heat bath (water molecules).

of rescaling the particle velocities is done by the thermostat. Due to the lower density, the water molecules will not be able to shield the ionic charges effectively any longer and particle formation of the ionic species takes place. The result is a strong temperature increase due to conversion of potential energy into kinetic energy. The temperature of the different species and of the whole system is calculated from the atomic and molecular velocities. The temperature increase after the change in state conditions can be seen in Figure 2a, which shows the time development of the system temperature for three different systems during the first 45 ps and in the long time limit. After a strong increase during the first few picoseconds the temperature approaches the target value as the newly formed particles get cooled by the surrounding water molecules, which are coupled to the thermostat. Figure 2b shows the time development of the average water temperature and the temperatures of the two ionic species together with the system temperature for a single simulation run. The water temperature reaches the target temperature of the thermostat very quickly after the change to the new state conditions while the ionic temperatures lag behind in their decrease (see the close up in the inset in Figure 2b). This is due to the fact that per collision between a water molecule and ion or forming salt cluster, only a limited amount of energy can be transferred to the water molecules which are coupled to the thermostat. For the rest of the duration of the simulation runs, the temperatures remain around the target temperatures and only show their typical fluctuations, which are larger for the ionic species because their number is smaller compared to the number of water molecules.

Figure 2c shows the time development of the system pressure as running averages for the same systems as in Figure 2a. The pressure is calculated from both atomic and molecular virials during the simulations.[25]After the change to the new state conditions the pressure increases first very fast and then a little slower to the resulting value of around 25 MPa. Figure 2d also shows the pressure vs time but for three systems at the same heat bath temperature but at different system densities. The pressures reach their equilibrium values on more or less the same time scale as the temperature. In Figure 2d, one can see that the different system density values result in pressures around 22.5 MPa for 0.13 g/cm^3 and around 28.5 MPa for 0.18 g/cm^3 at 835 K.

Radial distribution functions (RDF) $g(r)$, giving a measure of the probability to find an atom in a certain distance to a reference atom, have been obtained from the configurations of the last 50 ps (250 configurations) of each simulation run. It is the nature of radial distributions functions of those species, which exist in cluster form, to approach the long distance value of 1.0 much slower than if they are in the dissolved in the gas phase or a thin solution. The reason is the larger probability to find another ion at this distance for a reference ion located in a cluster with a diameter of 1 nm, for example, compared to the situation where ions are dissolved in a thin solution. In addition to the most interesting part of the RDFs up to a distance of 1 nm we therefore also show the long distance behavior in the diagrams in Figure 3 to prove the correct normalization of the curves.

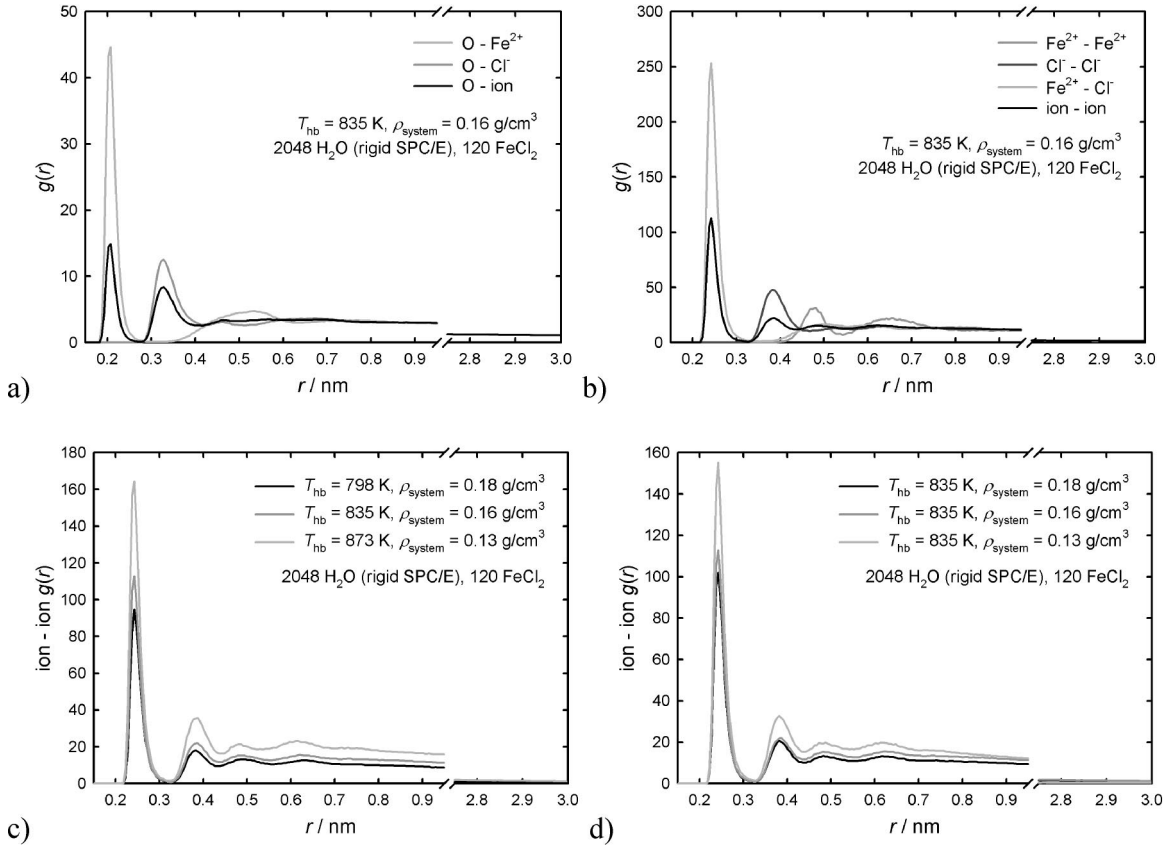

Figure 3. (a) Radial oxygen–ion distribution functions for one simulated system at $T_{hb} = 835$ K and 0.16 g/cm^3; (b) Radial ion−ion distribution functions for the same system as in part a. (c) Radial ion−ion distribution functions for simulation runs at three different state points. (d) Same as part c but for three systems at the same heat bath temperature but different system densities. Temperatures given in the legends are the temperature of the heat bath (water molecules).

Figure 3a shows radial distribution functions between the oxygen atom of the water molecules and the two different ionic species as well as a combined oxygen-ion RDF of a selected system. The first peak of the O−Fe^{2+} curve is located at 0.207 nm which is also the value found for all other systems investigated. The first minimum is located at approximately 0.32 nm and the next wide peak is likely to contain two peaks at around 0.45 and 0.54 nm. The first peak in the O−Cl^- RDF is located at 0.327 nm in all studied systems. The first minimum usually lies at 0.43 nm and the second maximum at 0.458 nm. A very shallow second minimum follows and a very wide third peak starts at around 0.6 nm. There is no clear temperature or density dependency of the peak location seen for any of these curves.

A typical picture of the ionic RDFs is given in Figure 3b. The ion−ion RDF has its first peak (which is the first Fe^{2+}−Cl^- peak) always at 0.243 nm, the first minimum at 0.325 nm and the second peak (which is also the first Cl^-−Cl^- peak) at 0.383 nm. The third peak in the combined ion−ion RDF lies at the first peak of the Fe^{2+}−Fe^{2+} RDF at 0.475 nm. The second peak of the Fe^{2+}−Cl^- RDF shifts from 0.6 nm in the system with the highest temperature and lowest density toward 0.5 nm in the system with the lowest temperature and highest density. In the systems at 835 K and 0.13 g/cm^3 the second maximum of this curve is very wide and ranges from 0.508 to 0.63 nm again containing probably two peaks. The Cl^-−Cl^- RDFs for the same systems also show a wide maximum ranging from 0.51 to 0.78 nm. This behavior probably stems from a very disordered structure in the salt particles formed in the supercritical water. The second peak in the Fe^{2+}−Fe^{2+} RDF is also subject to a shift from 0.65 to 0.64 nm when going from high temperature and low density to low temperature and high density. There is no such trend for the second Cl^-−Cl^- peak which lies at 0.52 nm in all investigated systems except the one mentioned above with the wide second maximum.

Figure 3c shows ion−ion RDFs for systems at three different state points. With increasing temperature and decreasing system density the peaks become more pronounced and have higher values. This is a hint toward a stronger structure formation at the state point at 873 K and 0.13 g/cm^3. The RDFs in Figure 3d are for systems at the same temperature of 835 K but different system densities. It can be clearly seen, that the trend to more pronounced peaks and higher peak values goes with decreasing system density.

Parts a−c of Figure 4 show snapshots[45] of the system configurations after 250 ps. In these as well as in all other investigated systems, all 360 ions have aggregated into one large cluster or very few smaller clusters. No single ions, ion pairs or even $FeCl_2$ molecules can be found throughout the systems. It is easy to see, that the water molecules, displayed as red and white sticks, not only surround the irregular shaped and disordered particles but can also be found in the interior between the ions. This is expected as it is known that $FeCl_2$ crystals grown from saturated aqueous solution contain crystal water and are called iron(II) chloride tetrahydrate ($FeCl_2 \cdot 4H_2O$).[46] These water molecules have to be taken into account when analyzing cluster sizes by means of the Stillinger criterion. The distances used in these analyses are given in Table 2 and correspond to the related minima of the RDFs.

Figure 5a shows the number of ions in the largest cluster within a system vs time for three different systems at three different state points. Only the Stillinger criteria for group one

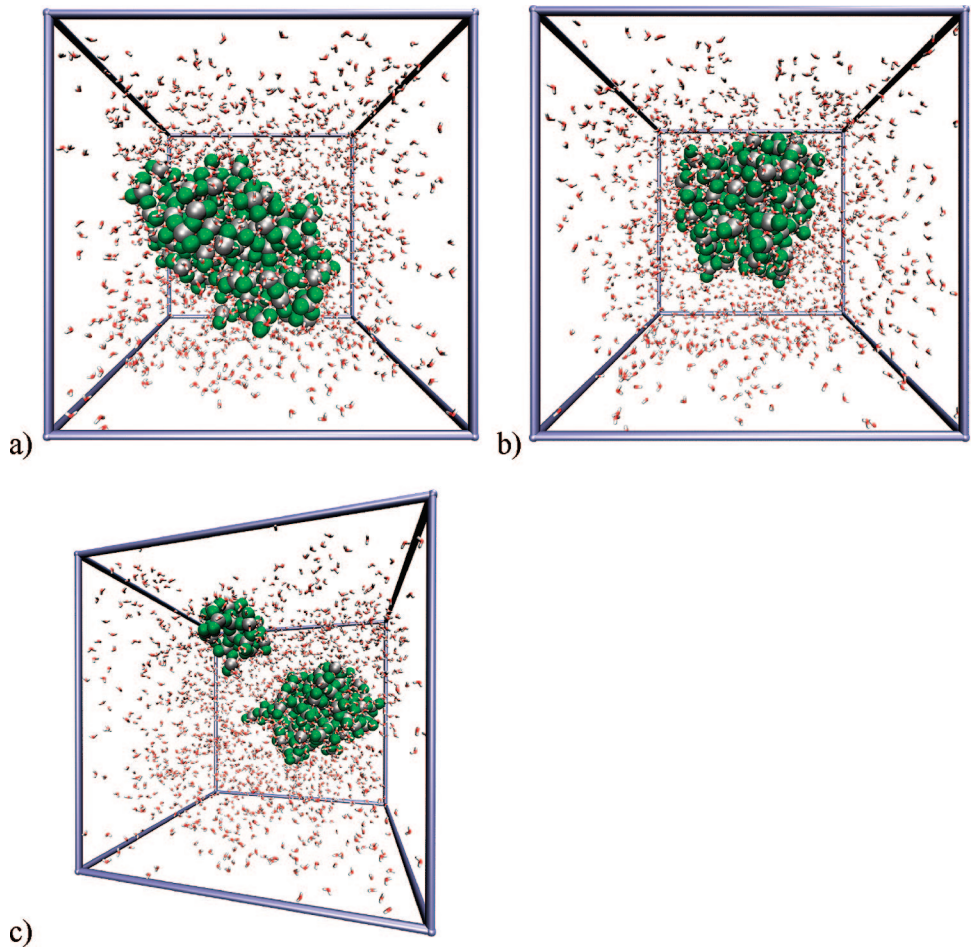

Figure 4. Snapshots of the last configuration (after 250 ps simulation time) for the system at (a) $T_{hb} = 798$ K and 0.18 g/cm^3; (b) $T_{hb} = 835$ K and 0.16 g/cm^3; and (c) $T_{hb} = 873$ K and 0.13 g/cm^3. All three configurations show crystal water between the ions in the clusters which is in agreement with water present in $FeCl_2$ clusters grown in aqueous solutions.[46]

TABLE 2: Stillinger Criteria for the Detection of Clusters

group no.		distance/nm
1. ions only	$Fe^{2+}-Fe^{2+}$, $Fe^{2+}-Cl^-$, Cl^--Cl^-	0.3225
2. ions and water molecules	$O-Fe^{2+}$	0.32
	$O-Cl-$	0.43
	$O-O$	0.38

(ions with ions only) were used in the cluster size analysis. Although all curves display aggregation and cluster growth to some extent, there are large fluctuations in the size of the largest cluster, sometimes up to 100 ions from one stored configuration to the next. But most importantly the cluster size and the cluster size distribution does not match the visualizations which show single clusters of size 360 ions or few large clusters. It is clear at this point that the water molecules have to be taken into account in marking which ions belong to a cluster. Figure 5b shows the growth curves for the same systems as in Figure 5a but now also marking two ions as belonging to the same cluster, if a water molecule (here taken as its oxygen atom) lies within a certain distance of both ions (Stillinger criterion group 2 in Table 2). The ion aggregation and cluster growth can be seen much clearer from doing the analysis in this way which can be justified by the knowledge of the water molecule inclusion within the aggregated particles by visual analysis using vmd.[45] Now the cluster sizes fit into the picture obtained from the visualization of the corresponding system configurations. Figure 5b furthermore shows, that aggregation and cluster growth happen very fast and most of the growth is finished after 30 to 50 ps. After that, all ions have aggregated already into a few large or one single cluster. The collisions of two clusters can be seen as large steps in the growth curves. Sometimes a collision and aggregation of two large clusters does not happen in a single step but over a very short period of time, where water molecules between the two colliding particles hinder a direct connection of the two collision partners. This then leads to an apparent decay of a just-aggregated cluster pair. But the final merging into one cluster is then usually just a matter of time, often only a few picoseconds at the given conditions. One can also see in Figure 5b, that the growth of the largest cluster is faster for the system at lower temperature and higher density. A close up on he first 50 ps of Figure 5b also reveals that the curves rise relatively smooth during the first 10−15 ps which is a hint toward growth by attachment of monomers or small entities like $Fe^{2+}-Cl^-$ pairs or $FeCl_2$ units. As many small clusters are formed in this way cluster growth switches over to a stochastic growth by cluster−cluster collisions resulting in the larger steps in the growth curves.

Figure 5c shows the temperature development of the largest clusters in Figure 5b. The cluster temperature is very large at the beginning. As already mentioned for the system temperature, this stems from the potential energy transformation into kinetic energy during the ion aggregation. Due to the weak coupling to the heat bath by collisions with the surrounding water molecules the clusters heat up significantly over the heat bath temperature. It is this heating up that causes the whole system

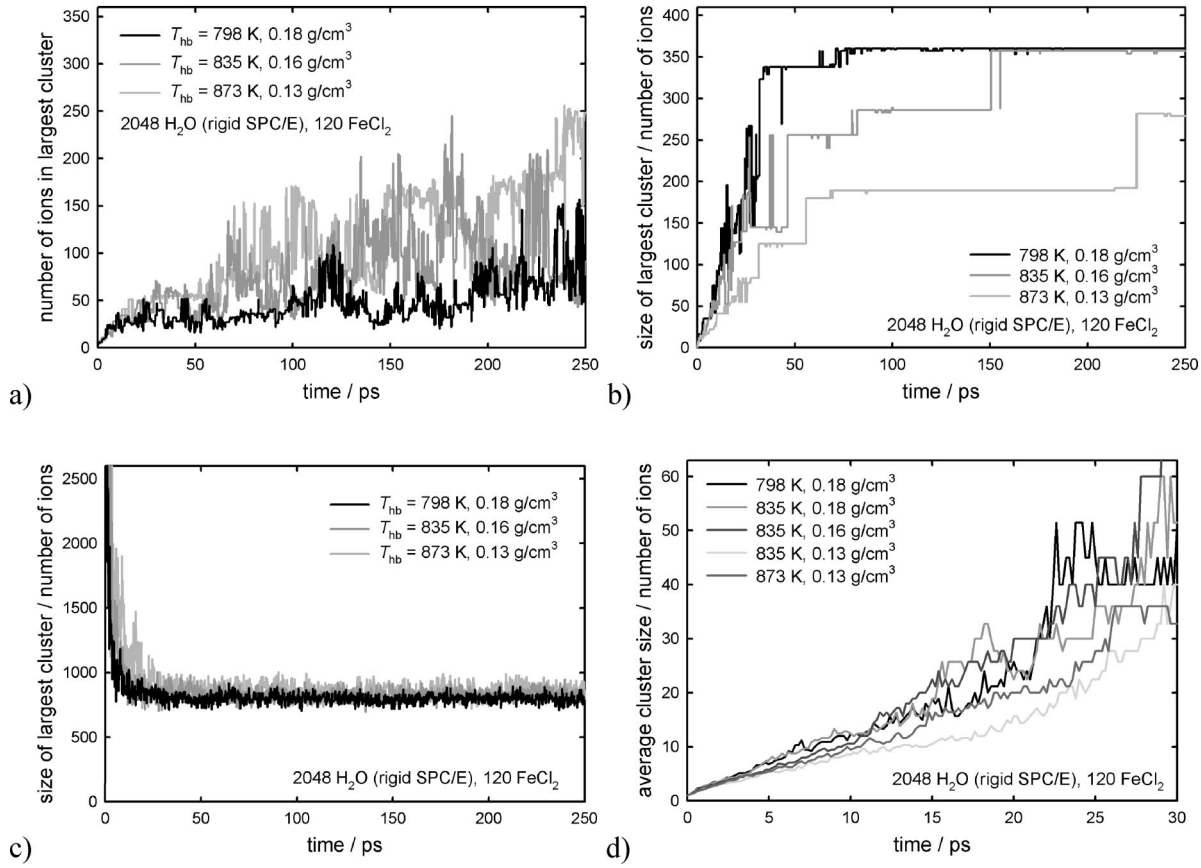

Figure 5. (a) Growth curves showing the number of ions in the largest cluster for single simulation runs at three different state points. (b) Growth curves of the largest cluster for the same systems as in part a but this time taking into account that water molecules function as bridges between the ions. Only the number of ions per cluster is counted, not the number of water molecules being part of it. (c) Temperature of the largest cluster in a system for three different simulation runs at different state points. (d) Average cluster size for five simulation runs at different state points. Temperatures given in the legends are the temperature of the heat bath (water molecules).

temperature to be larger than the target value of the heat bath thermostat in the first few tens of picoseconds of the simulations as already seen in Figure 2a.

To answer the question how heat bath temperature and system density affect the speed of the initial cluster growth we have plotted the average cluster size vs time in Figure 5d for simulations at the five different state points. The average cluster size is slightly larger for lower temperature and higher density for the first 10 ps. Then this behavior changes slightly as the curve for the system at 835 K and 0.16 g/cm^3 shows a sudden small increase. But it is typical for such plots that there are such crossovers of the different curves between 10 and 15 ps. Obviously, the growth mode changes during this time frame from adding monomers to trimers to existing clusters toward growth by collisions of larger clusters. From the trend of the curves after 15 ps it can also be seen, that the further growth is still slower at high temperature and low density compared to the situation at lower temperature and high density. This situation is the same in the plots of the same data of the other sets of simulation runs.

An interesting property of the growing aggregates is their composition. We here investigate this by plotting the Fe^{2+} mole fraction vs time in Figure 6a. It shows, that the systems' Fe^{2+} mole fraction of 1/3 is also reflected in the one of the largest cluster already after a very short time of a few picoseconds. The values stay in the range between 0.3 and 0.5 with only very few exceptions in the initial short time interval in some of simulated systems. The ideal value of $^1/_3$ is usually approached from the Fe^{2+}-rich side first and the curves show some fluctuations to both smaller and larger values around $^1/_3$ with ongoing growth. This is also why we have only plotted the first 30 ps of these curves. Furthermore, there is no trend to be seen in this behavior with heat bath temperature or system density.

When plotting the composition of the largest cluster vs its size one can also see the approach of the ideal Fe^{2+} content (Figure 6b). For small cluster sizes the majority of data points lies at or above $^1/_3$. This can be seen in Figure 6, parts c and d. At larger cluster sizes they appear to be distributed equally around this value while converging to $^1/_3$ in the limit of large cluster size. In the close ups on the range of small cluster sizes in Figure 6, parts c and d, the numbers given next to the data points are the Fe^{2+}:Cl^- ratio. These diagrams show, that short-lived species can be found during cluster growth, that have a high positive to negative charge ratio of up to +6:−3 or even +10:−5, like in one of the systems in Figure 6d. It would show up in diagrams like Figure 6a if the largest cluster in the system would be strongly charge imbalanced for a longer time period. Figure 6d shows the composition of the largest cluster in three simulation runs at the same state point, at the highest heat bath temperature and lowest density. With decreasing heat bath temperature and increasing density we find fewer data points in the plotted range of small cluster sizes which is connected to the faster growth, hence, this range of cluster sizes is covered within shorter time by the largest cluster in these systems, leaving behind a smaller variety of cluster compositions in this size interval.

While important characteristics of cluster growth can be made from studying the largest cluster in the system, it is as well

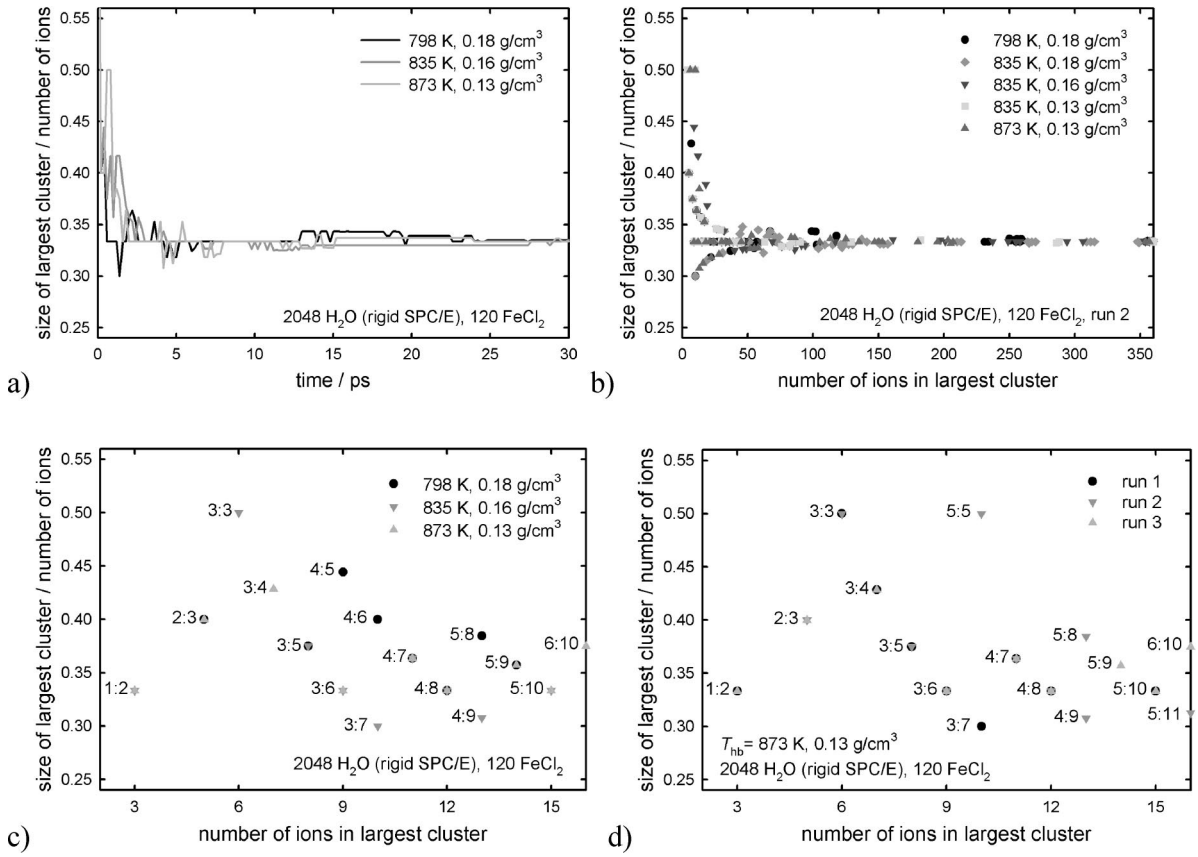

Figure 6. (a) Time development of the composition of the largest cluster for three simulation runs at different state points. Shown is the Fe^{2+} mole fraction of the largest cluster in a system. (b) Mole fraction of the largest cluster vs its size for three simulation runs at different state points. The captions at the data points mark the ratio of Fe^{2+}:Cl^- ions in the clusters. (c) Composition of the largest cluster vs cluster size for three simulation runs at different state points. (d) Same as part c but for another state point (T_{hb} = 873 K, 0.13 g/cm^3).

useful to study properties of the whole distribution of cluster sizes. In Figure 7 we have plotted three different properties for a simulation at 873 K and 0.13 g/cm^3. These are cluster size distribution (Figure 7a), cluster composition (Figure 7b) and cluster temperature (Figure 7c), averaged over 5 ps from 25 configurations for each partial plot per figure. Values for cluster sizes which do not appear in the given time intervals have been left out for clarity. In the first time interval (0−5 ps) mainly monomers, trimers, and small clusters up to nine ions in size exist with especially the monomers and trimers dominating the distribution. During the first shown time interval the clusters with four ions are mainly $Fe^{2+}-Cl^-_3$ clusters but there are also some $(FeCl)_2$ clusters present. The Fe^{2+} mole fraction shows values between 0.27 and 0.31 during the first 5 ps for this cluster size. If one assumes only $(FeCl)_2$ and $FeCl_3^-$ as possible tetramers, then there are at least 83% $FeCl_3^-$ tetramers in most of the systems, with only three systems showing lower values but not less than 74%. There seems to be a tendency to a higher amount of $FeCl_3^-$ in the systems with a system density of 0.13 g/cm^3. In the later time intervals this value is always at 0.25 with very few exceptions. This shows that the tetramers nearly always consist of one Fe^{2+} ion and three Cl^- ions.

The monomers more or less disappear during the second time interval (5−10 ps) and more clusters of sizes between 7 and 18 exist during this time. Taking a look at the average cluster composition during these two time intervals (Figure 7b) one can see, that the monomers are mainly Cl^- ions, pointing to the fact that the Fe^{2+} ions have already been built into dimers, trimers and larger aggregates. The sawtooth like distribution of data points in the second panel (5−10 ps) of Figure 7b is characteristic for all simulated systems. The deviations from it look like the curve in the first panel. The third and the fourth time interval of the cluster size distribution (Figure 7a) show how various cluster sizes disappear randomly from the distribution, marking the fact that collisions happen stochastically as clusters now grow by collisions with other clusters. Monomers and dimers are already completely gone from the distribution after 10 ps. The cluster sizes with the largest amount left are those with a size being an integer multiple of 3 and they all have the Fe^{2+} mole fraction of $^1/_3$ if they are present in the size distribution. The distribution of cluster compositions does not change with respect to the values, but only to the cluster sizes present in the size distribution. The distributions of cluster temperatures show how much the particles heat up during formation in the first time interval. The cooling down toward the heat bath temperature can already be seen in the second panel. Still some cluster sizes show elevated temperature. This can either come from heat set free during cluster−cluster collisions, or from the fact that a certain cluster size was only present for a short time in the given time interval. Then its temperature value could deviate from the heat bath temperature within the normal range of temperature fluctuations. Large deviations toward temperatures smaller than that of the heat bath are likely due to bad statistics due to very small number of clusters of this size present only for a very short time during the time interval in which the average was taken. Another reason might simply be, that these cooler clusters are biasing the overall system temperature to the value set by the thermostat, even if the thermostat is only coupled to the water molecules.

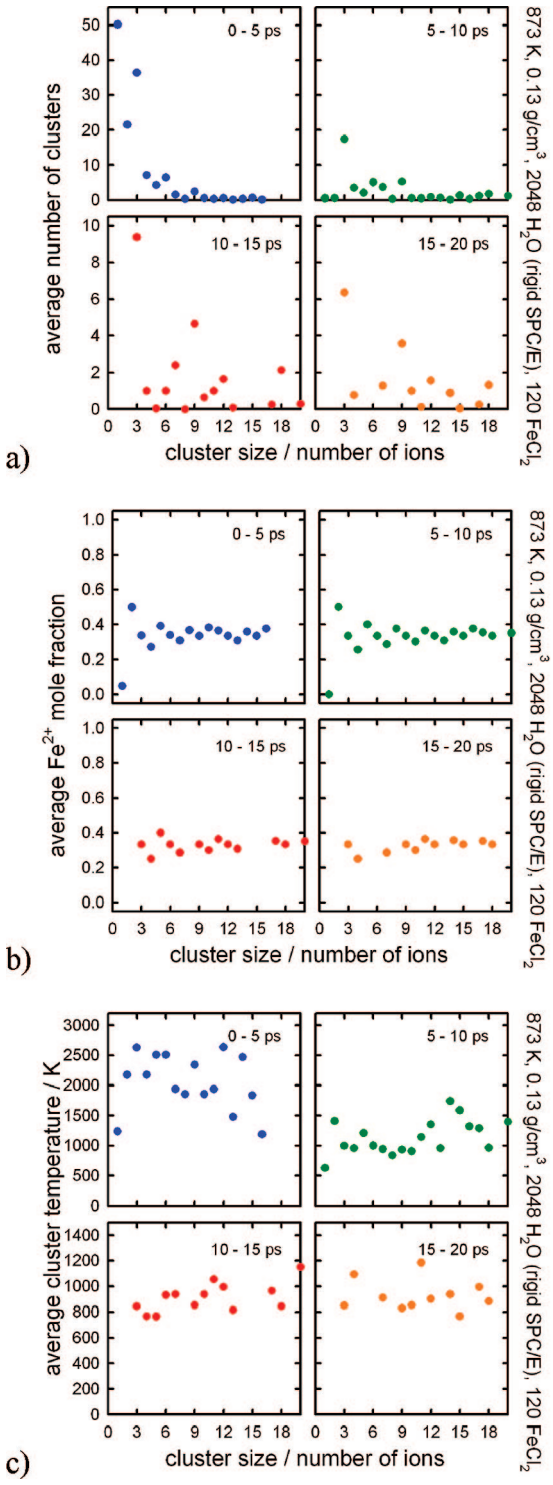

Figure 7. Cluster size and time averaged properties for a single simulated system at $T_{hb} = 873$ K and 0.13 g/cm^3. Shown are four 5 ps-time intervals for (a) cluster size distribution; (b) cluster composition by Fe^{2+} mole fraction; and (c) cluster temperature.

Discussion

The observed increase in temperature after the change from ambient to supercritical conditions due to particle formation is a well-known effect which has been reported through several publications. In one of these the heating up of newly formed particles has been observed by measurement of blackbody radiation in the gas phase production of iron nanoparticles,[47] and it is likely that this is also is the case during particle formation from supercritical water solution. As the investigated systems are quite low in density compared to the situation at ambient conditions it was decided to model the weaker coupling to the heat bath by the chosen heat bath thermostat. Application of a homogeneous thermostat to the nucleating species is known to lead to false dynamics, and corresponding unrealistic particle structures in case of strong interactions and intermediate or weak coupling among the atoms or molecules within a system.[33] Both conditions are given here with the low densities between 0.13 and 0.18 g/cm^3 and the strong Coulomb interaction due to the (partial) charges. The advantage of a heat bath thermostat compared to a homogeneous thermostat is that the amount of heat set free is removed locally and not throughout the whole system. The latter can lead to undesired repetitive and continuous cooling of monomers and very small clusters until their velocity becomes zero.[33] Use of a flexible interaction model for water could lead to a lower increase of the ionic species' temperatures during particle formation since additional energy can be stored in intramolecular vibrations in the water molecules. A study on differences between rigid and flexible model for the solvent is in progress.[48] The development of the system pressure follows closely that of the temperature as it very quickly rises from 0.1 MPa to the pressure corresponding to the given system density within about the first 10 ps. As the pressure is calculated from the virial and with that from the forces between the involved ions and water molecules, one can already see here, that the particle formation happens very fast and is more or less complete within very short time when the growth by cluster−cluster collisions is neglected.

Particle formation and growth could be followed in various ways. One method was to analyze the system for clusters by use of the Stillinger criterion and plotting the size and other properties of the largest cluster vs its size. The fact that the ionic aggregation takes place on the time scale of picoseconds is remarkable, but such high aggregation rates have also been found in other systems, including other ionic systems. Ohtaki and Fukushima[23] observed that particle growth was completed after 12−18 ps in their studies on dense NaCl and CsF solutions. From the results given in the work of Yang and Meng[49] on heterogeneous nucleation at the solid/liquid interface of a NaCl crystal and a NaCl containing solution it is possible to calculate a nucleation rate for NaCl clusters of 3 ions. From the number of stable clusters formed within 1200 ps one can calculate a nucleation rate of 10^{36} m^{-3} s^{-1}. Although there is a large gap in the state conditions between the study of Yang and Meng[49] (300 K system temperature, 1 bar system pressure) and ours, the rate of trimer formation is comparable to the values we obtained in our simulations both on NaCl[24] and $FeCl_2$[40] aggregation in supercritical water.

Concerning the fast speed of particle formation, the chosen system composition, e.g., the ion to water molecules ratio, is probably near but below the maximum value that leads to reasonable results although the employed weight fraction is not as extreme as in other studies.[19,23] While, from our experience, the number of ions should not be lower in investigations on growth and structure formation, an increase in the number of water molecules and thus a lower weight fraction of salts will lead to slower dynamics. A recent study on NaCl particle aggregation in supercritical water was published by Nahtigal et al.[50] in which relatively low 5.1 wt % salt solutions (ion: water 122:4000 = 0.03) were investigated. Nahtigal et al. chose to the same approach we used in our recent study[24] except for homogeneous thermostatting instead of the use of a heat bath thermostat. They obtained 2 orders of magnitude slower particle formation kinetics than we had observed in our investigation at

a larger salt weight fraction (20.2 wt %) and higher ion to water molecules ratio (0.156).

The different, well structured ion−ion RDFs show as well that ionic aggregation has taken place. The $Fe^{2+}-O$ peak at 0.207 nm lies between the two $Fe^{2+}-O$ distances for tetrahedral coordination (0.201 nm) and octahedral coordination (0.218 nm) determined by Apted et al.[51] They employed different methods of X-ray absorption spectroscopy on different Fe^{2+} and Fe^{3+} chloride solutions. The $Fe^{2+}-Cl^-$ peak at 0.243 nm also lies between the values for the two different coordinations which are the tetrahedral (0.238 nm) and the octahedral (0.258 nm) coordination. Neutron diffraction data of deuterated crystalline $FeCl_2 \cdot 4H_2O$ (iron (II) chloride tetrahydrate) obtained by Verbist et al.[52] shows the $Fe^{2+}-O$ distance at 0.209 to 0.212 nm in case of a perfect crystal structure (which is $P2_1/c$) and between 0.212 and 0.213 nm for a slightly distorted lattice. For the same type of distorted lattice, the $Fe^{2+}-Cl^-$ distance is found to be at 0.243 nm, which matches exactly our results. Verbist et al.[52] give the $H-Cl^-$ distance between 0.22 and 0.24 nm in the distorted lattice, which we find to lie around 0.235 nm. The comparison of experimental data and our results for the radial distributions functions are indications that the clusters contain water molecules, so-called crystal water, and that they are not yet relaxed into an ordered equilibrium ground-state structure within the simulation time covered.

The observation that the peaks of the ion−ion RDFs are more pronounced with decreasing system density could be related to less water molecules within the ionic clusters at higher temperature. The oxygen–ion RDFs also show at least two clear ionic peaks very close the oxygen atom and a well defined minimum between them, which is another hint to aggregated ions which are mostly in direct contact. The observation that interstitial water molecules play a role when it comes to applying the Stillinger criterion for detection of clusters can be seen from the system snapshots in Figure 4 and the comparison of the growth curves in Figure 5, parts a and b. If the water molecules that are neighbors to two or more ions are neglected the size of the largest cluster fluctuates very strongly and the size development is very slow. This is in contrast to the visual inspection through snapshots.[45] The possibility of a wrong choice of Stillinger criteria (too small values) through the inclusion of only the ionic species in this analysis can be ruled out. As the chosen distance criterion is the location of the minimum of the ion−ion RDF and its first peak is the $Fe^{2+}-Cl^-$ peak, there must be water molecules located between two ions of equal charge which are part of the same cluster. So the water molecules within the clusters or their surface must be accounted for when doing the Stillinger analysis. Mucha and Jungwirth[54] found water molecules within clusters of NaCl while they crystallized in water at ambient conditions. They were driven out of the clusters on a time scale of nanoseconds. It could be that the same is the case for the investigated $FeCl_2$ clusters and this is currently investigated in simulation runs lasting longer than a nanosecond of simulation time.[53] However, in view of the experimental investigation of $FeCl_2 \cdot 4H_2O$ crystals,[52] it is more likely, that the water molecules are an integral part of the $FeCl_2$ crystal and will not leave the clusters even on a much larger time scale.

Growth and structure development of clusters composed of oppositely charged colloids has been studied by Sanz et al.[55] Parallels can be drawn between our results and their conclusions on the degree of order of cluster structure attained during particle growth, which was neither the ground-state structure nor the one with the lowest free energy barrier of formation. Clusters which have just crossed the critical size limit for further growth are not in equilibrium with their surroundings in case of very fast growth processes. Such a situation is also found in our simulations. The large deviations of the cluster temperature over the heat bath temperature during the first stages of the nucleation and growth process are a clear sign for this. Rearrangement into a ground-state crystal structure at the given conditions before the next ions or other small clusters are attached to them is then just not possible. When the clusters are in equilibrium with the surrounding heat bath, the transition into an ordered crystal structure is then simply kinetically hindered and not observed on the time scale of our simulations. The observation of a two stage particle formation process by Shore et al.[21] supports this interpretation. They had also first observed a disordered crystal structure during and immediately after particle growth in their study on AgBr crystal growth.

When it comes to the initial stages of the ion aggregation, in which the clusters consist just of two or few more ions, the above definition of water molecules belonging to ionic clusters when they have at least two ions within a certain distance from their oxygen atom has an effect on the cluster size statistics. At the very beginning of the simulation existing solvent shared ions (pairs or triplets) are already counted as a dimer or trimer respectively. As a consequence the cluster size distribution can be nonzero for sizes of two or three ions already at the first time step but neglibly small compared to the number of monomers.

Even though clusters formed at higher heat bath temperature/lower system density appear to be more structured after the same simulated time, clusters aggregate faster at lower temperature/higher density. The latter has the stronger effect as the ions have a shorter way to each other and a higher probability for collisions than at lower density. Figure 5c shows that clearly for the three curves of average cluster size at 835 K heat bath temperature. The curves for the systems at 798 and 835 K and system densities corresponding to 25 MPa system pressure are very similar. But it is still observed that growth is slower at higher temperature and a density corresponding to the same system pressure.

Another influence of the water molecules on the properties of the small ionic clusters can be seen in the development of cluster composition with cluster size. The composition vs size of the largest cluster in Figure 6c and 6d shows that the cluster charge is unbalanced at small values. Fe^{2+}:Cl^- ratios of 3:3 and even 5:5 appear, which means charge ratios of $+6$:-3 and $+10$:-5. It is likely that the crystal water molecules have a stabilizing effect through partial shielding of the ionic charges from each other. A look into the histograms in Figure 7 also reveals that of the monomers, the Fe^{2+} ions are the first species to be completely built into aggregates. Their amount is already very close to zero within the first 5 ps (Figure 7b, upper left panel) although a considerable amount of monomers exists in this time interval (Figure 7a, upper left panel). While single clusters show partly strong unbalanced charge ratios the picture is smoother on the average, as can be seen from Figure 7b. Here, the Fe^{2+} mole fraction, and with it the charge ratio, stays as close as possible to the ideal value of $^1/_3$ with only minor deviations within the first 5 ps. The missing cluster sizes in the other time intervals are due to their depletion as they collide with other clusters and grow.

The development of cluster temperature shown for both the largest cluster in a system as well as averaged for short time intervals and plotted vs cluster size shows the source of heat that leads to the increase of the system temperature during the

phase of initial particle formation of surface growth or collisions of very small clusters of only a few ions. In Figure 7c, all clusters of all sizes that exists during the first presented time interval lie clearly above the heat bath temperature of 873 K. As particle growth is happening throughout the four time intervals shown only few clusters really equilibrate with the heat bath. While most cluster temperatures lie above that of the heat bath temperature, those cluster sizes with the largest occurrence during the respective time intervals show values close to the heat bath temperature. Sometimes, even significant deviations to values below the heat bath temperature can be observed, like for the monomers in the upper right panel of Figure 7c. There can be two reasons for such behavior. One can be bad statistics since the number of monomers is very small in this time interval. It is possible that a few monomers of a cluster of a certain size only existed for one or two of the 25 configurations from which the average values in the diagrams were calculated. It would have been possible to neglect cluster sizes which only exist for very few configurations but then one would lose information about interesting intermediate species, like for example the clusters with the large charge imbalances. The other reason for the temperature of small clusters lying below the heat bath temperature may be that they simply bias the other cluster temperatures which lie above the heat bath temperature to the observed average temperature. As shown in Figure 2b, the temperatures of the ionic species are at the temperature of the heat bath after about 15 to 20 ps. So the observed lower cluster temperatures after this point in time can be related to the mentioned biasing.

No trend of the development of cluster composition with temperature or density has been found. Even though Figure 6b could suggest that it is more likely to find compositions with a Fe^{2+}-mole fraction below $^1/_3$ at higher heat bath temperature/lower density, Figure 6d shows another picture for all three simulation runs carried out at this state point at 873 K and 0.13 g/cm^3. Also the time development of the cluster composition shows fluctuations around the ideal value of $^1/_3$ that appear more random than following a certain pattern. The picture is a bit different in the time averages over the different cluster sizes, in which a clear majority of $FeCl_3^-$ clusters were found, compared to $(FeCl)_2$ in the very early phase of ion aggregation.

Conclusions

We have conducted molecular dynamics simulations of the aggregation of $FeCl_2$ clusters in supercritical water at different state conditions between temperatures of 798 and 873 K and system densities from 0.18 g/cm^3 to 0.13 g/cm^3. New insight into the growth of $FeCl_2$ salt particles in supercritical water has been gained by following the growth and compositional development with time and cluster size. Particle growth is faster at lower temperatures and higher system densities. Water molecules are found to play an important role at this and later stages of particle growth, as they are found in considerable number within the salt particles. This is in agreement with crystal water present in $FeCl_2$ crystals grown from aqueous solutions ($FeCl_2 \cdot 4H_2O$). As small ion aggregates like $Fe^{2+}-Cl^-$, $Fe^{2+}-Cl^-_2$, and $Fe^{2+}-Cl^-_3$ etc. exist from the very beginning of the simulations growth by collision of these small entities and aggregation of ion monomers contribute most to the growth before collisions of larger clusters dominate once these small species are depleted in the systems. During the initial stages of particle growth, clusters with large charge ratios of up to +10:−5 are observed. However, on the average a Fe^{2+} mole fraction as close as possible to the ideal value of $^1/_3$ is found and with this a balanced ratio of ionic charges within the clusters. Even after 250 ps the clusters are found not to be in ordered crystalline structures. This can be explained by models of growth in which a cluster grows faster than its equilibration is possible before the addition of further monomers or growth by collision with another cluster. However, the comparison of the radial distribution functions taken during the last 50 ps of the simulation runs show good agreement with results from two different experimental techniques.

We are currently carrying out simulations on a longer time scale to investigate the structure formation within the particles and the role of the water molecules during the process. Furthermore, we are studying the same systems with different amounts of additional NaCl as well as the influence of flexibility in the interaction model for the water molecule.

Acknowledgment. This work was financially supported by the Deutsche Forschungsgemeinschaft (DFG) through a research scholarship (LU 1406/1-1) for N.L.

N.L. is grateful to T. Kraska from the Physical Chemistry Institute at the University in Cologne for stimulating discussions.

All simulations were carried out on the Linux cluster "fimm" at the Bergen Center for Computational Science (BCCS, http://www.bccs.uib.no) in Bergen, Norway.

References and Notes

(1) Bellissent-Funel, M.-C. *J. Mol. Liquid* **2001**, *90*, 313.
(2) Hodes, M.; Marrone, P. A.; Hong, G. T.; Smith, K. A.; Tester, J. T. *J. Supercrit. Fluids* **2004**, *29*, 265.
(3) Tester, J.; Holgate, H. R.; Armellini, F. J.; Webley, P. A.; Killilea; W. R.; Hong, G. T.; Berner, H.; E. Supercritical water oxidation technology. In *Emerging technologies in hazardous waste management III*; American Chemical Society: Washington, DC, 1993; pp 35−76.
(4) Aymonier, C.; Loppinet-Serani, A.; Reverón, H.; Garrabos, Y.; Cansell, F. *J. Supercrit. Fluids* **2006**, *38*, 242.
(5) Cansell, F.; Aymonier, C.; Loppinet-Serani, A. *Curr. Opinion Sol. Stat. Mater. Sci.* **2003**, *7*, 331.
(6) Kruse, A.; Dinjus, E. *J. Supercrit. Fluids* **2007**, *39*, 362.
(7) Kruse, A.; Dinjus, E. *J. Supercrit. Fluids* **2007**, *41*, 361.
(8) Marrone, P. A.; Hodes, M.; Smith, K. A.; Tester, J. W. *J. Supercrit. Fluids* **2004**, *29*, 289.
(9) Príkopský, K.; Wellig, B.; von Rohr, Ph. R. *J. Supercrit. Fluids* **2007**, *40*, 246.
(10) Lowell, R. P.; Rona, P. A.; Von Herzen, R. P. *J. Geophys. Res* **1995**, *100* (B1), 327.
(11) Von Damm, K. L.; Edmond, J. M.; Grant, B.; Measures, C. I.; Walden, B.; Weiss, R. F. *Geochim. Cosmochim. Acta* **1985**, *49*, 2197.
(12) Von Damm, K. L.; Edmond, J. M.; Measures, C. I.; Grant, B. *Geochim. Cosmochim. Acta* **1985**, *49*, 2221.
(13) Butterfield, D. A.; Jonasson, I. R.; Massoth, G. J.; Feely, R. A.; Roe, K. K.; Embley, R. E.; Holden, J. F.; McDuff, R. E.; Lilley, M. D.; Delaney, J. R. *Philos. Trans. R. Soc. Lond. A* **1997**, *355*, 369.
(14) Rona, P. A. *Science* **2003**, *299*, 673.
(15) Hovland, M.; Rueslåtten, H. G.; Johnsen, H. K.; Kvamme, B.; Kuznetsova, T. *Mar. Pet. Geol.* **2006**, *23*, 855.
(16) Hovland, M.; Kuznetsova, T.; Rueslåtten, H.; Kvamme, B.; Johnsen, H. K.; Fladmark, G. E.; Hebach, A. *Basin Res.* **2006**, *18*, 221.
(17) Sun, S.; Anders, S.; Thomson, T.; Baglin, J. E. E.; Toney, M. F.; Hamann, H. F.; Murray, C. B.; Terris, B. D. *J. Phys. Chem. B* **2003**, *107*, 5419.
(18) Sherman, D. M. *Geochim. Cosmochim. Acta* **2007**, *71*, 714.
(19) Harris, D. J.; Brodholt, J. P.; Harding, J. H.; Sherman, D. M. *Mol. Phys.* **2001**, *99*, 825.
(20) Berendsen, H. J. C.; Gridera, J. R.; Stratsmaa, T. P. *J. Phys. Chem.* **1987**, *91*, 6269.
(21) Shore, J. D.; Perchak, D.; Shnidman, Y. *J. Chem. Phys.* **2000**, *113*, 6276.
(22) Reagan, M. T.; Harris, J. G.; Tester, J. W. *J. Phys. Chem. B* **1999**, *103*, 7935.
(23) Ohtaki, H.; Fukushima, N. *Pure Appl. Chem.* **1991**, *63*, 1743.
(24) Lümmen, N.; Kvamme, B. *Phys. Chem. Chem. Phys.* **2007**, *9*, 3251.
(25) Lyubartsev, A. P.; Laaksonen, A. *Comput. Phys. Commun.* **2000**, *128*, 565.
(26) Stillinger, F. H. *J. Chem. Phys.* **1963**, *28*, 1486.

(27) Allen, M. P.; Tildesley, D. J. *Computer Simulation of Liquids*; Oxford University Press: Oxford, U.K., 1989.
(28) Berendsen, H. J. C.; Postma, J. P. M.; Van Gunsteren, W. F.; Di Nola, A.; Haak, J. R. *J. Chem. Phys.* **1984**, *81*, 3684.
(29) Andersen, H. C. *J. Chem. Phys.* **1980**, *72*, 2384.
(30) Nosé, S. *Mol. Phys.* **1984**, *52*, 255.
(31) Martyna, G. J.; Tobias, D. J.; Klein, M. L. *J. Chem. Phys.* **1994**, *101*, 4177.
(32) Kraska, T. *J. Chem. Phys.* **2006**, *124*, 054507.
(33) Erhart, P.; Albe, K. *Appl. Surf. Sci.* **2004**, *226*, 12.
(34) Westergern, J.; Grönbeck, H.; Kim, S.-G.; Tománek, D. *J. Chem. Phys.* **1997**, *107*, 3071.
(35) Wedekind, J.; Reguera, D.; Strey, R. *J. Chem. Phys.* **2007**, *127*, 064501.
(36) Yasuoka, K.; Matsumoto, M. *J. Chem. Phys.* **1998**, *109*, 8463.
(37) Römer, F.; Kraska, T. *J. Chem. Phys.* **2007**, *127*, 234509.
(38) Lümmen, N.; Kraska, T. *Eur. Phys. J. D.* **2007**, *41*, 247.
(39) Brodholt, J. P. *Chem. Geol.* **1998**, *151*, 11.
(40) Lümmen, N.; Kvamme, B. *J. Supercrit. Fluids* **2008**, DOI: 10.1016/j.supflu.2008.07.017.
(41) Ryckaert, J. P.; Cicotti, G.; Berendsen, H. J. C. *J. Phys. Chem.* **1977**, *23*, 327.
(42) Smith, D. E.; Dang, L. X. *J. Chem. Phys.* **1994**, *100*, 3757.
(43) Curtiss, L. A.; Woods Halley, J.; Hautman, J.; Rahman, A. *J. Chem. Phys.* **1987**, *86*, 2319.
(44) Babu, C. S.; Lim, C. *J. Chem. Phys. A* **2006**, *110*, 691.
(45) The snapshots have been made with the software "vmd" (visual molecular dynamics) by: Humphrey, W.; Dalke, A.; Schulten, K. *J. Mol. Graphics* **1996**, *14*, 33. It can be downloaded at http://www.ks.uiuc.edu/Research/vmd/.
(46) Thornton, D. D. *Phys. Rev. B* **1970**, *1*, 3193. McElearney, J. N.; Forstat, H.; Bailey, P. T. *Phys. Rev.* **1969**, *181*, 887.
(47) Freund, H. J.; Bauer, S. H. *J. Phys. Chem.* **1977**, *81*, 994.
(48) Lümmen, N.; Kvamme, B. Manuscript in preparation.
(49) Yang, Y.; Meng, S. *J. Chem. Phys.* **2007**, *126*, 044708.
(50) Nahtigal, I. G.; Zasetsky, A. Y.; Svishchev, I. M. *J. Phys. Chem. B* **2008**, *112*, 7537.
(51) Apted, M. J.; Waychunas, G. A.; Brown, G. E. *Geochim. Cosmochim. Acta* **1985**, *49*, 2081.
(52) Verbist, J. J.; Hamilton, W. C.; Koetzle, T. F.; Lehmann, M. S. *J. Chem. Phys.* **1972**, *56*, 3257.
(53) Lümmen, N.; Kvamme, B. Manuscript in preparation.
(54) Mucha, M.; Jungwirth, P. *J. Chem. Phys. B* **2003**, *107*, 8272.
(55) Sanz, E.; Valeriani, C.; Frenkel, D.; Dijkstra, M. *Phys. Rev. Lett.* **2007**, *99*, 055501.

JP710156B